The Visual Computer manuscript No.
(will be inserted by the editor)

Visual Simulation of Mixed-motion Avalanches with Interactions Between Snow Layers

Yusuke Tsuda · Yonghao Yue · Yoshinori Dobashi · Tomoyuki Nishita

Abstract In the field of computer graphics, simulation of fluids, including avalanches, is an important research topic. In this paper, we propose a method to simulate a kind of avalanche, *mixed-motion avalanche*, which is usually large and travels down the slope in fast speed, often resulting in impressive visual effects. The mixed-motion avala- nche consists of snow smokes and liquefied snow which form an upper *suspension layer* and a lower *dense-flow layer*, respectively. The mixed-motion avalanche travels down the surface of the snow-covered mountain, which is called *accumulated snow layer*. We simulate a mixed-motion avalanche taking into account these three snow layers. We simulate the suspension layer using a grid-based approach, the dense-flow and accumulated snow layer using a particle-based approach. An important contribution of our method is an interaction model between these snow layers that enables us to obtain the characteristic motions of avalanches, such as the generation of the snow smoke from the head of the avalanche.

Keywords Simulation · Fluids · Avalanche · Generation of snow smoke · Adhesion of snow smoke · Snow entrainment

1 Introduction

In the field of computer graphics, simulation of natural phenomena is one of the most important research topics. Among various natural phenomena, avalanches need to be simulated by computer graphics because of the difficulties to take photographed images and videos.

Y. Tsuda · Y. Yue · T. Nishita
The University of Tokyo
E-mail: {tsuday, yonghao, nis}@nis-lab.is.s.u-tokyo.ac.jp

Y. Dobashi
Hokkaido University
E-mail: doba@ime.ist.hokudai.ac.jp

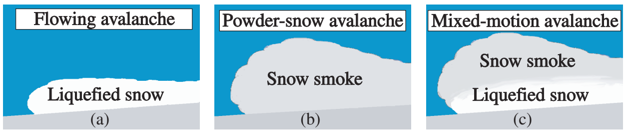

Fig. 1 (a) flowing avalanche, (b) powder-snow avalanche, and (c) mixed-motion avalanche.

Avalanches are classified into three categories: 1) flowing avalanches, 2) powder-snow avalanches and 3) mixed-motion avalanches [10] (see Figure 1). In this paper, we propose a method to simulate the mixed-motion avalanche.

The mixed-motion avalanche consists of two-tiered snow layers, called *dense-flow layer* and *suspension layer*, shown as Figure 1 (c). The dense-flow layer is the lower layer consisting of the snow which behaves like a liquid (such snow is called *liquefied snow*). The suspension layer is the upper layer consisting of snow smoke and air, covering the dense-flow layer. The snow on the surface of a snow-covered mountain, called *accumulated snow layer*, is also important for the motion of an avalanche, because the dense-flow layer usually entrains an accumulated snow layer, making the avalanche grow larger during the motion down the slope. Interactions between these three snow layers are important to obtain the motion of avalanche. An important contribution of this paper is an interaction model for the mixed motion avalanche between these snow layers.

In our method, the snow in the suspension and dense-flow layers are simulated as fluids. The dense-flow layer is about 100 times denser than the suspension layer [10]. We simulate the suspension and dense-flow layers as two-phase incompressible fluids for the stability of the simulation. The snow of the suspension layer and that of the dense-flow layer can be assumed to be the fluids with relatively small density differences, respectively [10]. This assumption is supported by the observations of real avalanches, as described in the literature [10].

The snow smoke in the suspension layer is simulated by a grid-based approach [16], because a number of particles are necessary to calculate the detail of the snow smoke [4]. On the other hand, the dense-flow layer is simulated by *Smoothed Particle Hydrodynamics*, SPH [5][12], because the dense-flow layer may undergo large deformations, such as the splash of the snow of the dense-flow layer when the dense-flow layer runs into obstacles.

In our method, we take into account two types of interactions: 1) interactions between the suspension and dense-flow layers and 2) interactions between the dense-flow and accumulated snow layers. Firstly, we assume that there is an *overlapping region with a high density contrast* between the dense-flow and suspension layers [10]. We assume that the overlapping region has non null thickness, and both the snow smoke and liquefied snow exist and interact with each other in the overlapping region. Secondly, we take into account snow entrainment: the dense-flow layer entrains the snow of the accumulated snow layer.

We show that our method can reproduce the characteristic phenomena of the mixed-motion avalanches observed in the real world, such as the generation of the snow smoke from the head of the avalanche.

2 Related Work

In the field of computer graphics, simulation models for the avalanches based on the physical properties of the snow layers have not been proposed to our knowledge. Kapler [8] created a computer-generated animation of an avalanche covered by snow smoke. In [8], snow smoke is represented by 3D volume texture attached to a series of rotating particles emitted from the head of an avalanche. In their results, the head of the avalanche moves through the air and emits the snow smoke in the air even though the head of the real avalanche usually moves on the ground and emit the snow smoke into the air.

In other research fields, *i.e.*, glaciology, physics, and computational geoscience, simulation models of avalanches have been proposed. However, no universal dynamic model has been established, and each proposed dynamic model is based on assumptions depending on categories of the avalanches. Previous simulation models for avalanches can be classified into following four types: center-of-mass models [13], granular flow models [14], depth-averaged models [7] and density current models [2].

Among these four models, center-of-mass models and old granular flow models cannot be used to calculate the shape and deformation of the avalanche, because the center-of-mass models and old granular flow models regard an avalanche as a simple mass point and a continuous body without deformation, respectively. The shape and deformation of the flowing avalanches can be calculated by granular flow models of recent years and depth-averaged models, and those of the powder-snow avalanches can be calculated by density current models. However, all of these four models cannot be used to simulate the mixed-motion avalanches because both the suspension and dense-flow layers are not taken into account. In our method, both these layers are taken into account, together with an interaction model between snow layers. The dense-flow layer is calculated by using particles as in the granular flow models. The suspension layer is calculated by using grid taking into account the influence of the air flow to the motion of the snow smoke, as in the density current models.

3 Previous Methods for Fluid Simulation

In this section, we briefly review grid-based and particle-based fluid simulation methods. The motions of the fluids are simulated by solving incompressible Navier-Stokes Equations:

$$\nabla \cdot \mathbf{u} = 0, \tag{1}$$

$$\rho\left(\frac{\partial \mathbf{u}}{\partial t} + (\mathbf{u}\cdot\nabla)\mathbf{u}\right) = -\nabla p + \mu\nabla^2\mathbf{u} + \mathbf{f}, \tag{2}$$

where $\mathbf{u}$ is the velocity, t is time, p is the pressure, ρ is the fluid density, μ is the viscosity and $\mathbf{f}$ is external forces.

3.1 Grid-based Method

In grid-based method [16], the quantities of the fluids, such as the velocity and density, are stored at fixed grid points, and the inflows and outflows of the quantities are calculated at each grid point. The velocities on grid points are updated by calculating Eq. (2), and a scalar quantitiy a is updated according to:

$$\frac{\partial a}{\partial t} = -(\mathbf{u}\cdot\nabla)a + \kappa\nabla^2 a + S, \tag{3}$$

where κ is the diffuse rate of the quantity and S is the increase or decrease of the quantity due to the external source.

3.2 Particle-based Method

In SPH [12], the motions of fluids are represented by the movement of particles. Each particle stores the position, velocity and mass. The motion of the fluid is simulated by following steps: 1) calculation of the densities of the fluid at the center of the particles, 2) calculation of the forces acting on particles, 3) update of the velocities and positions of the particles according to the calculated forces.

The density, pressure force and viscosity force of a particle are calculated based on the weighted influences on the

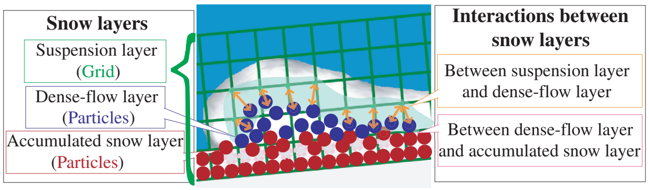

Fig. 2 Simulation model of a mixed-motion avalanche in the our method: Green mesh indicates a grid used in grid-based method. Blue and red circles indicate the SPH particles for the dense-flow layer and the accumulated snow layer, respectively. Orange arrows indicate interactions between dense-flow layer and suspension layer. The light green region indicates the overlapping region of the suspension and dense-flow layers. A part of the particles in the accumulated snow layer has moved from default position due to snow entrainment.

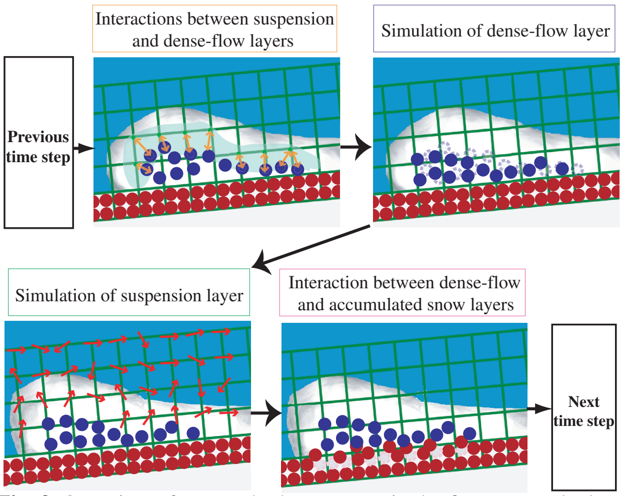

Fig. 3 Overview of our method: Processes in the figure are calculated in one time step. 1) Interaction forces between particles and grid points are calculated. 2) The motion of the dense-flow layer is calculated by SPH. 3) The motion of the suspension layer is calculated by a grid-based approach. 4) Snow entrainment is calculated.

particle from neighboring particles. In SPH, a scalar or vector quantity $\mathbf{A}(\mathbf{r})$ at the position $\mathbf{r}$ in the fluid is calculated as the weighted sum of the quantity $\mathbf{A}_i$ of the neighboring particle i:

$$\mathbf{A}(\mathbf{r}) = \sum_i m_i \frac{\mathbf{A}_i}{\rho_i} W\left(|\mathbf{r} - \mathbf{r}_i|, h\right), \tag{4}$$

where m_i is the mass of the particle i, ρ_i is the density of the particle i, W is a smoothing kernel function calculating the weight of influence on a particle from a neighboring particle, according to the distance between these two particles. h is used as the radius of support for weight calculation, and its value is constant and is same for all the particles. The density, pressure force and viscosity force of particle i are calculated by using Eq. (4). The smoothing kernels used to calculate these quantities are introduced in [12].

4 Proposed Method

Figure 2 shows the simulation model of our method. We simulate the motion of the suspension layer using a grid-based approach, and the dense-flow and the accumulated snow layers using a particle-based approach. Additionally, we introduce an interaction model between the snow layers. We take into account the interactions between the suspension layer and the dense-flow layer, and the interactions between the dense-flow layer and the accumulated snow layer. We ignore the interaction between suspension layer and the accumulated snow layer. The interactions between the suspension layer and the dense-flow layer are assumed to occur in the overlapping region (described in detail in Section 4.1), and such interactions include the generation and adhesion of the snow smoke and the interaction forces acting in the overlapping region. As the interactions between the dense-flow layer and the accumulated snow layer, we consider the snow entrainment. Figure 3 shows the flowchart of the processes calculated in a single time step.

In the following sections, we first define the overlapping region in Section 4.1. Then, we describe the details of the simulation of the suspension layer in Section 4.2, and dense-flow and accumulated snow layers in Section 4.3. We describe the interactions between snow layers in Section 4.4. Finally, we describe the initial conditions to start the simulation in Section 4.5.

4.1 Definition of the Overlapping Region

Since there is no contact surface between the suspension and dense-flow layers, we do not use previous methods for the multi-phase fluids, such as [6], which are designed to simulate the shapes and motions of the contact surfaces of the fluids. Instead, we introduce a concept of *overlapping regions*, in which both of the snow smoke of the suspension layer and the liquefied snow of the dense-flow layer exist, and the snow of these two layers interact with each other. The overlapping regions are defined as the region where the number densities of the particles are relatively low compared to those in the dense-flow layer. The number density $n(\mathbf{x})$ at position $\mathbf{x}$ is calculated by Eqs. (5) and (6) [9].

$$n(\mathbf{x}) = \sum_j W_n\left(|\mathbf{r}_j - \mathbf{x}|, h\right), \tag{5}$$

$$W_n(r,h) = \begin{cases} \frac{h}{r} - 1 & (0 \le r < h) \\ 0 & (r > h), \end{cases} \tag{6}$$

where W_n is a kernel function for particle number density, r is the distance between particles j and position $\mathbf{x}$, and h is the radius of support for weight calculation. If $n(\mathbf{x})$ is positive and lower than a threshold n_0, we regard position x to be in the overlapping region. Figure 4 shows an example of the classification of the particles in the dense flow layer.

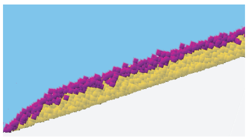

Fig. 4 Classification of the particles. The particles of the dense-flow layer traveling down the slope are shown without the snow smoke of the suspension layer. Particles in the overlapping region are shown in purple color, and the other particles are shown in yellow color.

4.2 Details of the Simulation of Suspension Layer

In our method, each grid point stores the velocity, the fluid density and the ratio r_s of the snow smoke density to the total density:

$$r_s = \frac{\rho_{smoke}}{\rho_{air} + \rho_{smoke}}, \tag{7}$$

where ρ_{air} is the density of the air, and ρ_{smoke} is the density of the snow smoke. The fluid density ρ in Eq. (2) is the total density of the snow smoke and the air, *i.e.*, $\rho = \rho_{smoke} + \rho_{air}$. We substitute r_s for a in Eq. (3) when solving Eq. (3). External forces acting on grid points are calculated by Eq. (8).

$$\mathbf{f} = \rho\mathbf{g} + \mathbf{f}^{buoyancy} + \mathbf{f}^{drag} + \mathbf{f}^{lift} + \mathbf{f}^{conf}, \tag{8}$$

where $\mathbf{g}$ is a gravitational vector, $\mathbf{f}^{drag}$ and $\mathbf{f}^{lift}$ indicate the interaction forces on a grid point from neighboring particles. $\mathbf{f}^{drag}$ is the force that makes particles move along with the flow on the neighboring grid points, and acts as an air resistance force on the particle. $\mathbf{f}^{lift}$ is the force that makes the particle move according to the vortices (see Section 4.4.1 for details). $\mathbf{f}^{buoyancy}$ is the buoyancy acting on snow smoke, and is calculated by Eq. (9).

$$\mathbf{f}^{buoyancy} = -(1 - r_s)\rho\mathbf{g}. \tag{9}$$

$\mathbf{f}^{conf}$ is an external force used to generate vortices calculated by vorticity confinement [3].

Next, we describe the boundary condition for the suspension layer. The boundary for the suspension layer is defined as the boundary between the accumulated snow layer and suspension layer, and between the overlapping region and the region of the dense-flow layer out of the overlapping region (see Figure 5). We find grid points that are on the boundary, as follows. Firstly, we find grid points that are obviously out of the boundary. These grid points are the ones that meet at least one of the following conditions:

(1) The grid point is the nearest to more than one particles of the dense-flow layer, and all of these particles are in the overlapping region.
(2) The grid point is not the nearest grid point to any of the particles.

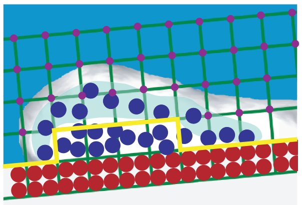

Fig. 5 Yellow line indicates the boundary for the suspension layer, and light green region indicates the overlapping region. Purple points indicate the grid points determined to be out of the boundary, and grid points on the yellow line are the grid points on the boundary.

Secondly, we treat a grid point as on the boundary when the grid point is not out of the boundary and one or more adjacent grid points are out of the boundary. We let the boundary condition be that the normal component of the velocity to the boundary is zero.

4.3 Details of the Simulations of Dense-Flow and Accumulated Snow Layers

In our method, each SPH particle stores its position, velocity and mass of the snow. As external forces, a gravitational force and reaction forces of $\mathbf{f}^{drag}$ and $\mathbf{f}^{lift}$ in Eq. (8) from the neighboring grid points are applied to the particles.

The particles of the accumulated snow layer are not allowed to move initially, and begin to move when the particles meet the condition for snow entrainment (see Section 4.4.2 for details). After a particle of the accumulated snow layer begins to move, the particle is treated as a particle of the dense-flow layer.

Figure 3 shows the flowchart of the processes calculated in a single time step.

4.4 Interactions between Snow Layers

Firstly, we introduce interactions between the dense-flow layer and suspension layer: generation of the snow smoke, adhesion of the snow smoke and interaction forces. In the overlapping region, the snow of the dense-flow layer is blown up and becomes snow smoke. On the other hand, the snow smoke adheres to the dense-flow layer. In this paper, we call these phenomena "generation of the snow smoke" and "adhesion of the snow smoke", respectively. Addition to these interactions, the fluids in the suspension and dense-flow layers push each other in the overlapping region through the interaction forces.

Secondly, we introduce snow entrainment as the interaction between the dense-flow and accumulated snow layers. The snow of the accumulated snow layer is entrained by that of the dense-flow layer and the total mass of the avalanche increases. Snow entrainment influences the size and speed of the avalanches and the deformation of the surface of the accumulated snow layer.

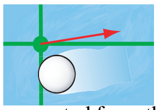

Fig. 6 The snow smoke is generated from the particle according to the relative velocity, indicated by the red arrow. The snow smoke is shown by blending white color with the background.

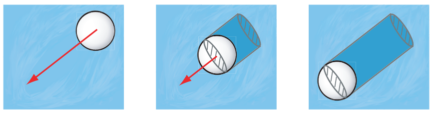

Fig. 7 The movement of the particle and adhesion progress is shown from left to right. Red arrow indicates the movement of the particle according to the relative velocity of the particle to the grid point. Diagonal lines indicate the sectional area of the particle.

4.4.1 Interactions between Suspension and Dense-flow Layers

As the forces between particle and grid point, we used coupling forces as described in Eqs. (10) and (11) [11].

$$\mathbf{f}_{i,j}^{drag} = -k_{drag}\frac{m_i}{r_i}|\mathbf{v}_i - \mathbf{u}_i|(\mathbf{v}_i - \mathbf{u}_i), \quad (10)$$

$$\mathbf{f}_{i,j}^{lift} = -k_{lift}m_i(\mathbf{v}_i - \mathbf{u}_i) \times \omega_i, \quad (11)$$

where $\mathbf{f}_{i,j}^{drag}$ and $\mathbf{f}_{i,j}^{lift}$ are the forces acting on particle i from grid point j, and k_{drag} and k_{lift} are constants. As the values of k_{drag} and k_{lift}, we used 0.81 and 0.2, respectively. m_i, r_i and $\mathbf{v}_i$ are the mass, radius and velocity of the particle i. $\mathbf{u}_i$ is the velocity at the position of the particle i interpolated from neighboring grid points. ω_i is the vorticity at the particle i. ω_i is interpolated from the vorticities of neighboring grid points, and vorticity of grid point j is calculated by $\omega_j^g = \nabla \times \mathbf{u}_j^g$, where $\mathbf{u}_j^g$ is the velocity of the grid point j. Forces acting on a grid point from particles are calculated as the reaction forces of $\mathbf{f}_{i,j}^{drag}$ and $\mathbf{f}_{i,j}^{lift}$.

To simulate generation of the snow smoke, a part of mass of the particle in the overlapping region is transferred to the neighboring grid point. Although the size of a particle should change according to the mass transfer, we currently fix the size of the particle and change its mass, instead. The amount of the transferred snow is related to the relative velocity of the particle to the grid point as shown in Figure 6. According to a real-world measurement [17] of the relationship between the wind velocity and the density blown from the surface of the accumulated snow layer, we model the amount G_j of generated snow smoke on the grid point j Eq. (12).

$$G_j = \sum_i C_g|\mathbf{u}_j - \mathbf{v}_i|^{1.7}S_i^{sur}\Delta t, \quad (12)$$

where C_g is a constant, $\mathbf{u}_j$ is the velocity on the grid point j, $\mathbf{v}_i$ is the velocity of the particle i neighbor to the grid point j, and S_i^{sur} is the surface area of the particle i. The user can specify the amount of the snow smoke by determining the value of C_g. In our method, we used 0.2 as the value of C_g according to [17].

We model the adhesion of the snow smoke based on the idea that each particle in the overlapping region sweeps the region, and the snow smoke in the swept region adheres to the particle. We calculate the amount A_i of the snow adhered to the particle i, using Eq. (13), based on the intuition that the amount of adhesion is related to the swept volume.

$$A_i = \sum_j C_a d_j S_i^{sec}|\mathbf{u}_j - \mathbf{v}_i|\Delta t, \quad (13)$$

where C_a is a user-specified constant, and we used 0.2. d_j is the density of the snow smoke on the grid point j neighbor to the particle i, and S_i^{sec} is the sectional area of the particle i. In Eq. (15), $S_i^{sec}|\mathbf{u}_j - \mathbf{v}_i|\Delta t$ indicates the volume swept by the particle in a single time step.

4.4.2 Interactions between Dense-flow and Accumulated Snow Layers

As the interactions between dense-flow and accumulated snow layers, we take into account snow entrainment. We ignore the effect that snow in the dense-flow sticks onto the accumulated snow layer. In the snow entrainment process, the particles of the dense-flow layer entrain the particles from the accumulated snow layer. We determine whether each particle of the accumulated snow layer is entrained or not, according to the result of the experiment on the fracture of the accumulated snow [18]. In [18], relationship between fracture of the accumulated snow and the strain rate (defined as the change in strain over the time) of the snow is researched, and threshold of strain rate for the fracture of the accumulated snow is obtained.

In our method, particles of the accumulated snow layer are entrained when the calculated strain rate of each particle is greater than a threshold γ_0 obtained from [18], which ranges from 0.000001 to 0.0001 exponentially to the depth at the particle from the surface of the accumulated snow layer. The strain rate γ_i is calculated based on the relationship between strain rate of snow and the mass the snow is sustaining [10]:

$$\gamma_i = \frac{1}{\eta}W_i\sin\theta + \gamma_f, \quad (14)$$

$$\eta = 8.5 \times 10^6\exp(0.021\rho_a), \quad (15)$$

where η is the viscosity coefficient of the accumulated snow, and W_i is the total mass of the snow of the dense-flow and accumulated snow layers on the top of particle i [10] (see Figure 8). We ignore the masses of the air and the snow of the suspension layer because they are negligible. θ is the angle of the slope, and γ_f is the strain rate due to friction. ρ_a

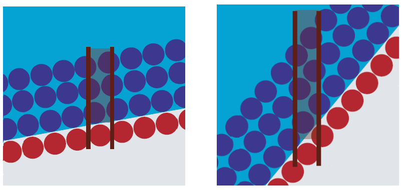

(a) (b)

Fig. 8 Blue and red circles indicate the particles of the dense-flow layer and the accumulated snow layer, respectively. A particle of the accumulated snow layer receives the total mass of the snow in the light brown region. The accumulated snow layer receives more mass of the snow in the vertical direction when the slope is (a) more steeply inclined than (b) gently inclined.

is the density of the accumulated snow layer. As the value of ρ_a, we used observational value ($100kg \cdot m^{-3}$). Eq. (15) is obtained from measurements [10] and indicates the relationship between the viscosity coefficient and density of the accumulated snow. The value of η is usually large and γ_i is close to the threshold γ_0.

As described above, the determination of the snow entrainment whether a particle i of the accumulated snow layer is entrained or not is based on the comparison between γ_i and γ_0. However, if we conduct this determination at each time step, the result will be affected by the time step Δt: smaller Δt will result in more times of the determination and more snow will be entrained when Δt is smaller. To resolve this problem, we conduct the determination not at every time step but in a certain probability P_e at each time step, which is calculated as:

$$P_e = \frac{Er}{\bar{m}} \cdot \Delta t \cdot S^{sec}, \tag{16}$$

where Er is the observational mass value of the entrained snow from a $1m^2$ surface of the accumulated snow layer per one second, $10(kg \cdot m^{-2} \cdot s^{-1})$ [15]. $\bar{m}$ is the initial mass of a single particle of accumulated snow layer. S^{sec} is the sectional area of the particle. Strictly speaking, P_e is not linear to Δt, but can be approximated as Eq. (16) if P_e is sufficiently small, as shown in Appendix A. Each particle of the accumulated snow layer is treated as a particle of the dense-flow layer after the particle is entrained.

4.5 Initial Conditions

The placement of the particles in the accumulated snow layer should be arranged in order not to make the simulation unstable when a particle of the accumulated snow layer is entrained: if the distance between two particles are too small, a strong force acts between two particles and makes the simulation unstable. We arrange the particles of the accumulated snow layer to meet two conditions: 1) the particles are arranged nearly uniformly, 2) the average distance between two nearest neighbor particles is the same as the value of the initial particle distance of the dense-flow layer particles. To meet these conditions, we first determine the initial positions of the particles by using pseudo random numbers so that these particles are arranged nearly uniformly. Then, these particles are iteratively moved to be arranged more uniformly by using a relaxation method [19].

We set the velocities and densities on grid points to zero (which can be set arbitrary according to user's demand). The particles of the dens-flow layer are set on the top of the slope.

5 Results

Section 5.1 shows the results of 2D simulation, and Section 5.2 shows the results of 3D simulation. Simulations are conducted on a PC with Intel Core 2 DUO 3.33 GHz CPU. Δt is determined in an adaptive way according to CFL condition [1].

5.1 Results of 2D Simulation

In 2D simulation, a vertical cut of an avalanche is calculated. The resolution of the grid is 690×240. The number of particles in the dense-flow layer increased from 1,000 to 2,800 on an average, due to the snow entrainment. Memory usage is about 40MB. Grid spacing is $0.33m$, and the influential radius of the particles is $0.21m$. Each simulation consists of about 2,400 time steps, and the average computational time for one time step is about 80 ms.

In the results shown in Figures 9, 10, 11 and 12, particles of the dense-flow layer are shown with white color, and the snow smoke is shown by blending white color with the background color according to the ratio of snow smoke density ρ_s on a grid point. The simulation time is shown in the upper left corner of each result image, and the scale of length is shown in the lower right.

Figure 9 (a) shows the result of the simulation of an avalanche traveling down a bumpy slope. The number of the particles of the dense-flow layer increased from 1,000 to 2,560 by snow entrainment. Characteristic phenomena of the mixed-motion avalanches that are often observed in the real world, such as the rounded shape of the section of the avalanche head, long tail of the avalanche, and swirling snow smoke are reproduced simultaneously. Figures 9 (b) and (c) show the simulation results of avalanches traveling down the steeply and gently inclined slope, respectively. By snow entrainment, the number of particles of the dense-flow layer increased from 1,000 to 3,700 in (b), and from 1,000 to 2,040 in (c). More particles are entrained from the accumulated snow layer when the slope is inclined more steeply because the accumulated snow layer receives more weight of the snow (see Figure 8). The avalanche on the steeply inclined slope travels down the slope at high speed. Therefore, the air resistance force on the dense-flow layer is strong and

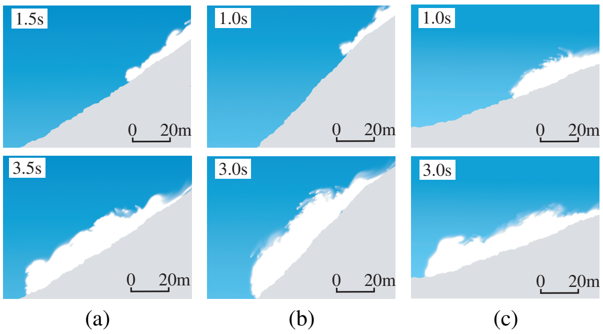

Fig. 9 Avalanches travelling down differently inclined slopes.

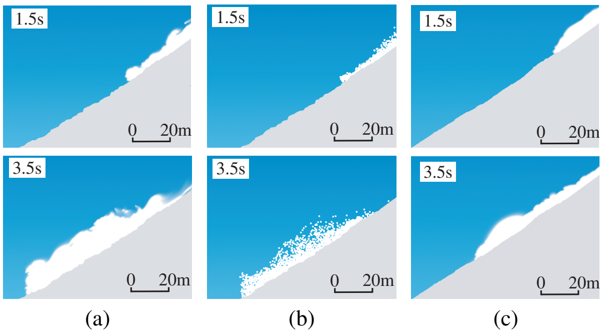

Fig. 10 Comparison of the effects of the interactions. (a) Simulation with generation, adhesion of snow smoke and interaction forces. (b) Simulation with interaction forces but without generation and adhesion of snow smoke. (c) Simulation with generation and adhesion of snow smoke but without interaction forces.

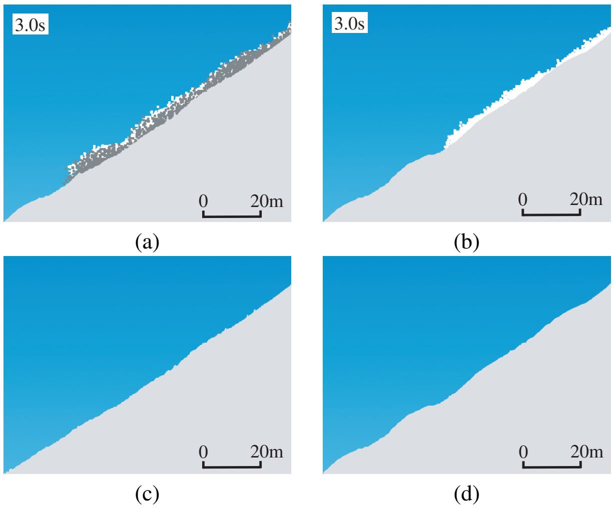

Fig. 11 (a) The result of the simulation with snow entrainment. (b) The result of the simulation without snow entrainment. (c) and (d) The accumulated snow layers after the avalanches in (a) and (b) passed.

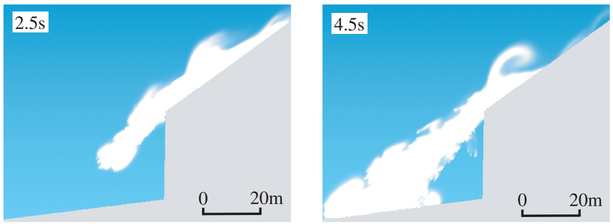

Fig. 12 An avalanche falling off the cliff in 2D simulation.

the amount of the snow smoke generation is large, resulting in the thick avalanches, as shown in (b). On the other hand, the avalanche on the gently inclined slope travels down the slope at low speed, resulting in the thin snow layers because of weak air resistance force and small amount of snow smoke generation.

Figure 10 shows the comparison of the effects of the interactions between the suspension and dense-flow layers. Figure 10 (a) is the result of the simulation with generation, adhesion of snow smoke and interaction forces. Figure 10 (b) shows the result of the simulation with interaction forces but without the generation and adhesion of the snow smoke. The characteristic motion of the snow smoke, such as the generation from the head of the avalanche and swirling motions, are not seen in (b). Therefore, the simulation without taking into account snow smoke is not suitable for the mixed-motion avalanche. Figure 10 (c) shows the result of the simulation with generation and adhesion of snow smoke but without interaction forces. Compared to Figure 10 (a), the shape of the snow smoke of the suspension layer is too simple. Therefore, the interaction forces are also important.

In Figure 11, the results of the simulations with (a) and without (b) snow entrainment process are shown. In (a) and (b), the particles of the dense-flow layer at the same simulation time are shown without snow smoke. White particles indicate the particles of the dense-flow layer when the simulation starts, and the dark gray particles indicate the particles entrained from the accumulated snow layer. As shown in (a), the avalanche becomes larger by snow entrainment. The avalanche in (a) travels down the slope faster than the avalanche in (b), which agrees with the fact that larger avalanche travels down the slope faster [10]. (c) and (d) show the accumulated snow layers after the avalanches of (a) and (b) have traveled down the slopes, respectively. The surface of the accumulated snow layer in (c) is smoother than that in (d) because the surface snow of the accumulated snow layer is entrained in (c).

Figure 12 shows the result of the simulation of an avalanche falling off a cliff. During falling, the snow smoke is generated from the head of the avalanche, and the head does not spread because of air resistance. The snow in the head of the avalanche is then pushed by the snow falling from the cliff.

5.2 Results of 3D Simulation

In 3D simulation, the resolution of grid is $30 \times 40 \times 170$, and the number of particles of the dense-flow layer is increased from 10,000 to 22,000 by snow entrainment. Grid spacing is $1.0m$, and influential radius of the particles is $0.21m$. Memory usage is about 200 MB. Whole simulation

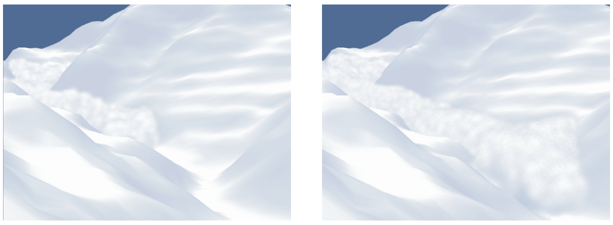

Fig. 13 An avalanche traveling down the slope in 3D simulation.

consists of about 3,000 time steps, and the average computational time for a single time step is about 8 seconds.

Figure 13 shows the result of our method in 3D. An avalanche is traveling down a slope of a mountain. Characteristic phenomena of the mixed-motion avalanche, such as the generation of the snow smoke from the head of the avalanche, are reproduced.

6 Conclusions and Future Work

In this paper, we have presented a simulation method for mixed-motion avalanches taking into account snow layers and interactions between snow layers. The suspension layer is simulated by a grid-based approach, and the dense-flow and accumulated snow layers are simulated by a particle-based approach. We calculated interactions between the suspension and dense-flow layers and snow entrainment. We showed that our method can simulate the characteristic phenomena of the mixed-motion avalanches observed in the real world, such as the generation of the snow smoke from the head of the avalanche.

As future work, we would like to use rendering techniques taking into account light scattering by snow for realistic rendering of avalanches. Moreover, we would like to reduce computational time by using GPU and more efficient representation for the suspension layer, *e.g.*, adaptive grids.

Acknowledgements We gratefully acknowledge helpful comments and thoughtful suggestions from the anonymous reviewers. We would also like to thank Dina Systems Co., Ltd. for providing the terrain data of Mt. Myoko for 3D simulation. The second author is supported by Grant-in-Aid for JSPS Fellows (20・7968).

References

1. R. Courant, K. Friedrichs, and H. Lewy. On the Partial Difference Equations of Mathematical Physics. *IBM Journal*, pages 215–234, 1967.
2. J. Etienne, M. Rastello, and E. J. Hopfinger. Modelling and Simulation of Powder-Snow Avalanches. *C. R. Mechanique 334*, pages 545–554, 2006.
3. R. Fedkiw, J. Stam, and H. W. Jensen. Visual Simulation of Smoke. *Proc. of SIGGRAPH2001*, pages 390–399, 2001.
4. Y. Gao, Li, S. C. Hu, and B. A. Barsky. Simulating Gaseous Fluids with Low and High Speeds. *Pacific Graphics 28*, pages 1845–1852, 2009.
5. R.A. Gingold and J.J Monaghan. *Mon. Not. R. Astron. Soc.*, 181, 375.
6. J. Hong and C. Kim. Discontinuous Fluids. *Proceedings of ACM SIGGRAPH 2005*, pages 915–920, 2005.
7. K. Hutter, M. Siegel, S. B. Savage, and Y. Nohguehi. Two-Dimensional Spreading of a Granular Avalanche down an Inclined Plane part I. Theory. *Acta Mechanica 100*, pages 37–68, 1992.
8. A. Kapler. Avalanche! snowy FX for XXX. *SIGGRAPH 2003 Sketches and Applications, 2003*, 2003.
9. S. Koshizuka and Y. Oka. Moving Particle Semi-Implicit Method for Fragmentation of Incompressible Fluid. *Nuclear Science and Engineering 123*, pages 421–434, 1996.
10. N. Maeno, Y. Endo, E. Akitani, S. Kobayashi, and M. Takeuchi. *Avalanche and Snowstorm (Nadare to Fubuki)*. Kokonshoin, 2000 (in Japanese).
11. J. Magnaudet and I. Eames. The Motion of High Reynolds-Number Bubbles in Inhomogeneous Flows. *Annual Review of Fluid Mechanics 32*, pages 659–708, 2000.
12. M. Müller, D. Charypar, and M. Gross. Particle-Based Fluid Simulation for Interactive Applications. *Proc. of Siggraph Symposium on Computer Animation*, pages 154–159, 2003.
13. A. Perla. Avalanche Release, Motion, and Impact. *Dynamics of snow and ice masses*, pages 397–462, 1980.
14. B. Salm and H. Gubler. Measurement and Analysis of the Motion of Dense Flow Avalanches. *Annals of Glaciology 6*, pages 26–34, 1985.
15. B. Sovilla, S. Margreth, and P. Bartelt. On Snow Entrainment in Avalanche Dynamics Calculations. *Cold Regions Science and Technology 47*, pages 69–79, 2007.
16. J. Stam. Real-Time Fluid Dynamics for Games. *Proc. of the Game Developer Conference*, 2003.
17. M. Takeuchi. Vertical Profile and Horizontal Increase of Drift Snow Transport. *Journal of Glaciology 26*, pages 481–492, 1980.
18. M. Takeuchi. An Experimental Study on Tensile Fracture of Snow. *Institute of Low Temperature Science*, pages 1–37, 1983.
19. G. Turk. Generating Textures on Arbitrary Surfaces Using Reaction-Diffusion. *Proceedings of the 18th annual conference on Computer graphics and interactive techniques*, pages 289–298, 1991.

A Approximation on Probability of Snow Entrainment Calculation

As shown in Section 4.4.2, we approximate that P_e is linearly proportional to Δt. The derivation for the approximation follows the following steps. We first consider the following two cases: 1) the simulation proceeds with large time step Δt, 2) the simulation proceeds with small time step $\Delta t/m$ in m times, where m is a positive integer. Next, assuming the snow entrainment occurs (*i.e.*, the strain rate is greater than the threshold), we calculate the probabilities of a single particle of the accumulated snow layer being entrained during the time Δt in these two cases. In order to ensure the entrainment process not to be affected by the setting of the time step, these two probabilities should be the same. From this observation, we finally derive the relationship between P_e and the time step.

We first consider the first case. Assume that we conduct the determination of entrainment in probability P_1. Obviously, the particle is entrained during the time Δt in the probability P_1. Next, we consider the second case. Assume that we conduct the determination of entrainment in a single time step $\Delta t/m$ in probability P_m. Then, the particle is entrained during the time Δt in the probability Q_m, given as:

$$Q_m = P_m + (1-P_m)P_m + (1-P_m)^2 P_m + \cdots + (1-P_m)^{m-1} P_m. \quad (17)$$

This equation is obtained by simply summing up the entrainment probability at each time step, and simplifies to Eq. (18).

$$Q_m = 1-(1-P_m)^m. \quad (18)$$

When P_m is sufficiently small, which is the case in our simulation, Eq. (18) can be approximated as

$$Q_m \approx 1-(1-mP_m) = mP_m. \quad (19)$$

Since the probabilities of the particle being entrained during the time Δt in these two cases should be the same, we obtain

$$P_m \approx P_1/m, \quad (20)$$

which states that the probability P_m should be proportional to the time step.




YUSUKE TSUDA received the B.S. and M.S. degrees in Computer Science from the University of Tokyo, Japan, in 2008, and 2010, respectively. His research interests center in computer graphics including visual simulation.

YONGHAO YUE received the B.S. and M.S. degrees in Computer Science from the University of Tokyo, Japan, in 2005, and 2007, respectively. He is currently a doctoral student in the Department of Information Science and Technology at the University of Tokyo. His research interests center in computer graphics including photo-realistic rendering.

YOSHINORI DOBASHI is an associate professor at Hokkaido University in the graduate school of information science and technology, Japan since 2006. His research interests center in computer graphics including realistic Image synthesis, efficient rendering, sound modeling for virtual reality applications. Dobashi received his BE, ME and Ph.D in Engineering in 1992, 1994, and 1997, respectively, from Hiroshima University. He worked at Hiroshima City University from 1997 to 2000 as a research associate.

TOMOYUKI NISHITA received the B.E., M.E., and Ph.D. degrees in Electrical Engineering from Hiroshima University, Japan, in 1971, 1973, and 1985, respectively. He worked for Mazda Motor Corp. from 1973 to 1979. He has been a lecturer at the Fukuyama University since 1979, then became an associate professor in 1984, and later became a professor in 1990. He moved to the Department of Information Science of the University of Tokyo as a professor in 1998 and now is a professor at the Department of Complexity Science and Engineering of the University of Tokyo (since 1999). He received a Research Award on Computer Graphics from IPSJ in 1987, Steven A. Coons Awards from ACM SIGGRAPH in 2005, and a CG Japan Award in 2006. His research interest is mainly in computer graphics. He is a member of IEICE, IPSJ, ACM, and IEEE.